

Journal of Materials Chemistry C

Accepted Manuscript



This is an *Accepted Manuscript*, which has been through the Royal Society of Chemistry peer review process and has been accepted for publication.

Accepted Manuscripts are published online shortly after acceptance, before technical editing, formatting and proof reading. Using this free service, authors can make their results available to the community, in citable form, before we publish the edited article. We will replace this *Accepted Manuscript* with the edited and formatted *Advance Article* as soon as it is available.

You can find more information about *Accepted Manuscripts* in the [Information for Authors](#).

Please note that technical editing may introduce minor changes to the text and/or graphics, which may alter content. The journal's standard [Terms & Conditions](#) and the [Ethical guidelines](#) still apply. In no event shall the Royal Society of Chemistry be held responsible for any errors or omissions in this *Accepted Manuscript* or any consequences arising from the use of any information it contains.

Near Infrared-Emitting *Tris*-Bidentate Os(II) Phosphors: Control of Excited State Characters and Fabrication of OLEDs

Jia-Ling Liao,^a Yun Chi,^{a,*} Chia-Chi Yeh,^b Hao-Che Kao,^b Chih-Hao Chang,^{b,*} Mark A. Fox,^c Paul J. Low,^{d,*} and Gene-Hsiang Lee^e

^a Department of Chemistry and Low Carbon Energy Research Center, National Tsing Hua University, Hsinchu 30013, Taiwan; E-mail: ychi@mx.nthu.edu.tw

^b Department of Photonics Engineering, Yuan Ze University, Chungli 32003, Taiwan; E-mail: chc@saturn.yzu.edu.tw

^c Department of Chemistry, Durham University, South Rd, Durham, DH1 3LE, UK

^d School of Chemistry and Biochemistry, University of Western Australia, 35 Stirling Highway, Crawley, 6009, Western Australia, Australia; E-mail: paul.low@uwa.edu.au

^e Instrumentation Center, National Taiwan University, Taipei 10617, Taiwan

Abstract

A series of four Os(II) complexes bearing i) chromophoric diimine ligands (N[^]N), such as 2,2'-bipyridine (bpy) and substituted 1,10-phenanthrolines, ii) dianionic bipz chelate ligands derived from 5,5'-di(trifluoromethyl)-2H,2'H-3,3'-bipyrazole (bipzH₂), and iii) bis(phospholano)benzene (pp2b) as the third ancillary ligand completing the coordination sphere were synthesized. X-ray diffraction studies confirm the heteroleptic *tris*-bidentate coordination mode. These Os(II) complexes [Os(N[^]N)(bipz)(pp2b)], N[^]N = bpy (**3**), phenanthroline (**4**), 3,4,7,8-tetramethyl-1,10-phenanthroline (**5**) and 4,7-diphenyl-1,10-phenanthroline (**6**) display near infrared (NIR) emission between 717 nm to 779 nm in the solid state at RT. On the basis of hybrid-DFT and TD-DFT calculations, the emissions are assigned to metal-to-ligand charge transfers (³MLCT) admixed with small ligand-to-ligand

charge transfer (³LLCT) contributions. Successful fabrication of organic light emitting diodes (OLEDs) using Os(II) complex **5** as the dopant and either *tris*(8-hydroxyquinoline) aluminum (Alq₃) or 3,3',5,5'-tetra[(*m*-pyridyl)-phen-3-yl]-biphenyl (BP4mPy) as host is reported. These OLEDs were measured with emission maxima at 690 nm and extending into the NIR, with peak power efficiencies up to 0.13 lm/W and external quantum efficiencies up to 2.27%.

Introduction

Phosphorescent metal complexes have been extensively investigated during past two decades due to the profound interests in basic photophysics¹⁻⁹ and applications in organic light emitting diodes (OLEDs) suited for fabrication of flat panel displays¹⁰⁻¹³ and luminaires.¹⁴⁻¹⁹ As a consequence of the needs of these applications, many studies have focused on achieving bright visible emission, with colors spanning from blue and green to red. Another class of compounds being of great interest is the near infrared (NIR) emitting materials; i.e. those with emission peak maximum exceeding 700 nm.²⁰⁻²² NIR-emitting materials can find application in biological imaging, sensing and in optical tele-communications platforms. Among the various systems explored to date, Pt(II) complexes constitute a class of molecules that have shown the most efficient NIR emission,²³⁻²⁷ either through the use of chelating ligands with extended peripheral π -conjugation or by engineering strong π - π stacking interactions among molecules in the solid state for excimer formation. For example, electroluminescence with peak maximum at 772 nm and external quantum efficiency (EQE) of 5.0% was documented for a Pt(II) tetraphenyltetrabenzoporphyrin,²⁸ while the maximum EQE was further improved to 9.2% through the introduction of the 3,5-di-*tert*-butylphenyl substituted tetrabenzoporphyrin to control intermolecular interactions and suppress

triplet-triplet annihilation.²⁹

However, promising results in the area of NIR-emitting materials are not restricted to Pt(II) complexes, and both Ru(II) complexes with π -bonded (η^4 -) orthoquinone ligands,³⁰ Ir(III) complexes bearing cyclometalated heteroaromatics,³¹⁻³⁴ or with azabenz-annulated perylene bisimide³⁵ stand as illustrative examples of other metal-containing NIR-emitting materials. Parallel to this endeavor, we have developed Os(II) phosphors bearing isoquinolinyl azolate chelate ligands, which lower the emission energy gaps and bring emission into the NIR region.^{36, 37} The two Os(II) complexes [Os(bpy)(dttz)(CO)₂] (**1a**) and [Os(bpy)(dttz)(PPhMe₂)₂] (**2**) bearing both the neutral 2,2'-bipyridine (bpy) and dianionic 3,3'-bi-1,2,4-triazolate (dttz²⁻) chelating ligand also serve to demonstrate important molecular design features (Chart 1). In complex **2** due to the increase in electron density at the Os(II) metal center brought about by the phosphine co-ligands, we can take advantage of the combined metal-to-ligand charge transfer (MLCT) and the ligand-to-ligand charge transfer (LLCT) transitions to achieve NIR-emitting characteristics.³⁸

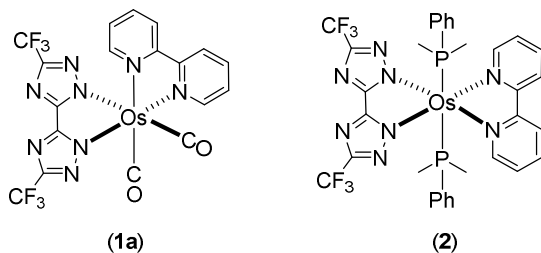


Chart 1: Reported Os(II) complexes **1a** and **2**.

To further explore the methodology to tune emission into the NIR region, we have designed heteroleptic *tris*-chelating Os(II) complexes containing i) bpy or 1,10-phenanthroline as the chelate with lower lying π^* -orbitals, ii) 5,5'-di(trifluoromethyl)-3,3'-bipyrazolate (bipz²⁻) as a dianionic, strongly electron donating chelate, and iii) 1,2-bis(phospholano)benzene (pp2b) as the third bidentate chelate to impose the formation of all *cis*-coordination geometry. The photophysical and structural characterization of the resulting NIR-emitting Os(II) complexes and the

device performance of the NIR-emitting OLEDs formed from these compounds are described here.

Results and Discussion

Syntheses and Characterization. It has been reported that the cluster complex $\text{Os}_3(\text{CO})_{12}$ reacts with functional pyrazoles (or triazoles) to form isolable intermediate derivatives via CO elimination.³⁹⁻⁴³ Subsequent sequential addition of Me_3NO and phosphines at elevated temperature led to the formation of mononuclear Os(II) complexes with diverse structures and distinctive photophysical properties. Such synthetic procedures were employed to prepare the aforementioned complexes *cis*-[Os(bpy)(dttz)(CO)₂] (**1a**) and phosphine substituted *trans*-[Os(bpy)(dttz)(PMe₂Ph)₂] (**2**).³⁸

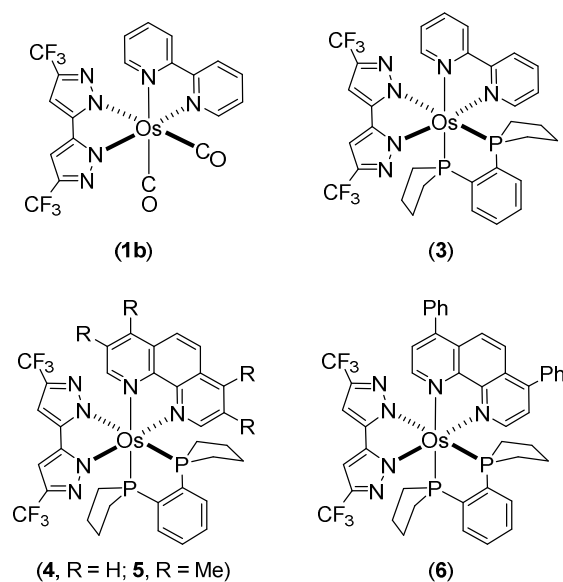


Chart 2: Os(II) complexes **1b** and **3** – **6** investigated in this study.

Here, this synthetic procedure was extended through reactions of $\text{Os}_3(\text{CO})_{12}$ with the distinctive dipyrazole pro-ligand 5,5'-di(trifluoromethyl)-2H,2'H-3,3'-bipyrazole (bipzH_2) and a range of diimine chelates ($\text{N}^{\wedge}\text{N}$ = bpy, phenanthroline (phen),

3,4,7,8-tetramethyl-1,10-phenanthroline (Me_4phen), and 4,7-diphenyl-1,10-phenanthroline (Ph_2phen) to give *cis*- $[\text{Os}(\text{bipz})(\text{N}^{\wedge}\text{N})(\text{CO})_2]$ (isolated by way of example for $\text{N}^{\wedge}\text{N} = \text{bpy}$, **1b**). Further reaction with anhydrous Me_3NO and 1,2-bis(phospholano)benzene (pp2b) gave the *tris*-heteroleptic complexes $[\text{Os}(\text{bipz})(\text{N}^{\wedge}\text{N})(\text{pp2b})]$ (**3 – 6**) (Chart 2).

However, the synthetic yields for **3 – 6** (21 ~ 35 %) are notably lower than that obtained for the *trans*-complex **2** (~ 50%). Varying the *cis*-diphosphine, such as 1,2-diphenylphosphinobenzene, failed to afford any isolable product, which is in contrast to previous reactions,⁴⁴ showing the delicate balance of structural and electronic effects imposed by the phosphines.

All of the new Os(II) metal complexes, i.e. **1b** and **3 – 6**, were purified by silica gel column chromatography and recrystallization, and then fully characterized by mass spectrometry, IR and NMR spectroscopies and elemental analyses. Multinuclear NMR spectra clearly established the heteroleptic nature of the complexes; for example, complex **3** showed two distinctive ^1H NMR singlet signals at δ 6.54 and 6.39 and two ^{19}F NMR signals at δ -59.62 and -59.65 assigned to the *bipz* chelate, characteristic multiplets from the *bpy* ligand, and two well separated ^{31}P NMR signals at δ 39.88 and 33.80 due to the coordinated *pp2b*. Therefore, these data clearly confirmed the presence of the three distinct chelating ligands coordinated to the Os(II) atom. Moreover, the IR $\nu(\text{CO})$ bands of the dicarbonyl complex **1b** were found at 1978 and 2040 cm^{-1} , which are located at lower wavenumbers than those of **1a** (i.e. 1994 and 2058 cm^{-1}) which contains the bis(triazolate) ligand, *dtz*.³⁸ This observation is in agreement with the greater electron donating character of *bipz*, and the increased back π -bonding which serves to reduce the CO stretching frequencies.

The structures of **1b** and **3** were determined by single crystal X-ray diffraction, for which a perspective view of each molecule, selected bond distances and angles are shown in Figures 1 and 2. Both Os(II) complexes adopt a distorted octahedral

geometry at the metal center, with the bpy and bipz chelates being located *cis* to each other, leaving two remaining *cis*-coordination sites that are occupied by two CO ligands (**1c**) or the pp2b chelate (**3**). In complex **1b**, the *trans*-influence of the CO ligands increases the *trans*-Os-N distances (i.e. Os-N(2) = 2.102(4) and Os-N(6) = 2.121(4) Å) versus those at the *cis*-dispositions, cf. Os-N(3) = 2.057(4) and Os-N(5) = 2.080(4) Å.³⁹ For the pp2b complex **3**, since both the *trans*-Os-N distances, i.e. Os-N(3) = 2.113(6) and Os-N(6) = 2.123(5) Å, are comparable to the *trans*-Os-N distances observed in **1c**, the *trans*-influence of pp2b chelate should be at the same magnitude as that imposed by dual CO ligands, despite of the large distinction in their intrinsic characters, i.e. σ -donor vs. π -acceptor.⁴⁵ Moreover, the bipz chelate in **3** adopts a subtly bent conformation, which contrasts to the near-planar arrangement of this ligand in **1b**. Since pp2b is more sterically bulky than the CO ligands, the associated crystal-packing effect, in part, likely influences this conformational distortion in the crystal lattice.⁴⁶

Photophysical data. Complex **1b** is non-emissive in both solution and solid states, so discussion of photophysical properties is focused only on the phosphine substituted Os(II) complexes **3** – **6**. For these complexes, UV-Vis absorption spectra were recorded in CH₂Cl₂ and the numerical data are presented in Table 1. As shown in Figure 3, the absorption spectra exhibit strong absorption bands below 320 nm ($\epsilon > 3 \times 10^4 \text{ M}^{-1}\cdot\text{cm}^{-1}$) assigned to $^1\pi\text{-}\pi^*$ transitions localized on the diimine ligands. The next, lower energy absorption in the region 400 ~ 500 nm ($\epsilon = 4 \sim 10 \times 10^3 \text{ M}^{-1}\cdot\text{cm}^{-1}$) is attributed to the spin-allowed $^1\text{MLCT}$ transitions from the Os(II) metal ion to the diimine. The intensities of these $^1\text{MLCT}$ bands show strong correlation to the nature of the diimine ligands; i.e. complexes **3** and **6** give the weakest and greatest intensity transitions which may be due in part to the degree of π -conjugation in the diimine acceptor. Moreover, there is a very broad absorption envelope that extends beyond 600 nm ($\epsilon = 1.2 \sim 2.1 \times 10^3 \text{ M}^{-1}\cdot\text{cm}^{-1}$), that can be assigned to the heavy-metal atom enhanced $^3\text{MLCT}$ absorption, and probably, mixed with the contribution from the

ligand-to-ligand charge transfer (³LLCT) transitions from the occupied orbital of bpy to the empty π^* -orbital of diimine chelate.

The Os(II) complexes **3** – **6** failed to show any notable emission in solution at RT, but were significantly emissive in the solid state, a result of the rigid media as well as the forfeit of solvent collision.^{47, 48} The solid state emission spectra and associated peak maxima (Figure 3) are sensitive to the nature of the diimine N^N chelate, supporting the assignment of the ³MLCT transition. For example, replacing bpy chelate in **3** with phen chelate in **4** leads to a blue shift of emission from 772 nm to 739 nm, which is due to the more destabilized π^* -orbital of phen versus bpy.⁴⁹⁻⁵² In a similar fashion, upon introduction of four methyl substituents (**5**) or two phenyl groups (**6**) to the phenanthroline ligand the corresponding emission maxima are blue shifted relative to the parent complex **4** to 717 nm and red shifted to 779 nm, respectively. These variations are attributed to the electron donating and extended π -conjugation for the methyl and phenyl substituents.

Complexes **3** - **6** showed emission quantum yields $\Phi = 0.5\% - 8.8\%$, and relatively short luminescence lifetimes at RT ($\tau_{\text{obs}} = 26.4 - 431$ ns) for phosphorescent processes. The radiative (k_r) and nonradiative decay (k_{nr}) rates were calculated from the Φ and τ data. The low Φ value of **3** is principally caused by the less rigid molecular framework of the bpy ligand, which then increases k_{nr} versus other Os(II) complexes with more structurally rigid phenanthroline-based chelates.⁵³ Within the series of phenanthroline complexes **4** – **6**, complex **5** showed higher Φ and longer τ_{obs} values versus those of parent **4**, which is best explained by the energy gap law,^{54, 55} i.e. k_{nr} values tend to increase as the emission energy decreases. In the case of complex **6** with the extended Ph₂phen chelate, the Φ value of 4.5% is higher than 3.1% of **4**, whilst τ_{obs} (115 ns) is comparable to that of parent complex **4** (197 ns). The derived k_r and k_{nr} values for **6** are calculated to be 3.91×10^5 and 0.83×10^7 s⁻¹, respectively. This could be due to the fact that, upon photoexcitation, the peripheral Ph substituents would become coplanar with the phenanthroline backbone, resulting in

more extended electron delocalization in the excited state.^{56,57} Therefore, the better electron delocalization produces a smaller variation in the C–C bond lengths upon formation of the excited state as compared to the ground state and, ultimately, giving the larger radiative quantum yield relative to other molecules in this class.⁵⁸

Electrochemistry. The electrochemical properties of **3** – **6** were examined using cyclic voltammetry (Table 2). The obtained data support the delineation that oxidation is localized on the Os(II) metal center, and that reduction occurs mainly on the diimine.⁵⁹ In the present system, all Os(II) complexes **3** – **6** showed reversible oxidation potential in the narrow range of 0.00 – 0.07 V (vs. the ferrocenium/ferrocene couple at 0.0 V), whilst the reduction potential was recorded between –2.04 and –2.30 V (cf. Table 2 and Figure S1 of supporting information). The trends in reduction potentials followed the trends anticipated on the basis of the electron donating or withdrawing character of the diimine ligands. Thus, changing from bpy to phen (i.e. from **3** to **4**) and addition of four methyl groups to phen (i.e. from **4** to **5**) result in destabilization of the empty π^* -orbital of diimine chelate, and a consequent shift in the reduction potential to more negative values. For **5**, the small decrease in oxidation potential versus **4** is also coupled with the increase in electron density at the metal center exerted by four methyl groups on phen. The possibility to create a more extended π^* system in the Ph₂phen complex **6** gives the least negative reduction potential when compared with the parent compound **4**.

DFT calculations. In order to gain in-depth insight into the above experimentally observed properties, we turned to calculations based on density functional theory (DFT) and time-dependent density functional theory (TD-DFT) (B3LYP / LANL2DZ basis set for Os, 6-31G** and all other atoms, as well as a conductor-like polarization continuum CPCM solvent model in CH₂Cl₂). The model structures are denoted **3'**, **4'**, **5'** and **6'** to distinguish them from the physical data of the as-synthesized complexes. The results from the geometry optimisations are summarised in Table 3, together with the crystallographically determined data from **3** for comparison. In the case of **3**

and **3'**, the majority of differences in bond lengths are within 0.03 Å, whilst the greatest difference is around 0.06 Å, associated with the Os-P(2) bond.

Plots of the HOMO and LUMO of **3'**, **4'**, **5'** and **6'** are given in Figure 4 and the supporting information. In each case the HOMO is of mixed Os(d)-bipz(π) character, (Os/bipz: 49/44 (**3'**); 48/45 (**4'**); 57/32 (**5'**); 49/44 (**6'**)) whilst the LUMO is strongly localized on the diimine ligand. The HOMO energies vary little across the series (Table 4) whilst the LUMO energies naturally follow the electronic characteristics of the diamine, giving good correlation with the redox potentials.

To provide a more detailed interpretation of the photophysical properties of **3 - 6**, time-dependent density functional theory (TD-DFT) calculations were also carried out. The results are summarized in Table 4, which lists the energy and orbital analyses of the lowest energy singlet and triplet transitions, together with the relevant data from the absorption and emission spectra. The agreement between the calculated $S_0 \rightarrow S_1$ transition energies are remarkably good, and although the $S_0 \rightarrow T_1$ transition is strictly forbidden and the calculations do not allow for spin-orbit coupling, the calculated transition energies (albeit with zero oscillator strength) follows the trend in emission maxima (Table 4). The $S_0 \rightarrow T_1$ transition energies may also account in part for the low energy tails observed in the absorption spectra (Figure 3). The simulated absorption spectra for the Os(II) complexes **3 - 6** are given in the supporting information (SI).

The $S_0 \rightarrow S_1$ and $S_0 \rightarrow T_1$ transitions are assigned to HOMO \rightarrow LUMO charge transfer processes, of mixed MLCT / LLCT character for each of **3'**, **4'** and **6'**. In the case of **5** which bears the Me₄-phen ligand, the $S_0 \rightarrow S_1$ transition also has appreciable HOMO \rightarrow LUMO+1 character (also MLCT / LLCT between the Os/bipz donor and diimine) whilst the $S_0 \rightarrow T_1$ transition is of mixed HOMO-1 \rightarrow LUMO / HOMO-2 \rightarrow LUMO character (again, largely MLCT / LLCT in nature).

OLED Device Fabrication. For OLED device fabrication, complex **5** was selected as

the dopant due to both the higher volatility and quantum yield compared with the other members of the series. In this study, tris(8-hydroxyquinoline)aluminum (Alq_3) and 3,3',5,5'-tetra[(*m*-pyridyl)-phen-3-yl]-biphenyl (BP4mPy), were used as both host and electron transport layer (ETL). The electron mobilities of Alq_3 and BP4mPy are recorded to be 10^{-5} and 10^{-4} cm^2/Vs , respectively.⁶⁰⁻⁶³ Moreover, 4,4'-bis[N-(1-naphthyl)-N-phenyl-amino] biphenyl (NPB) which possesses adequate hole transport mobility ($\sim 10^{-4}$ cm^2/Vs) and triplet energy gap ($E_T = 2.29$ eV) was selected as the hole transport layer (HTL) in tuning the carrier balance.⁶⁴⁻⁶⁶ The devices A1 and B1 consist of the architecture: ITO/ NPB (40 nm)/Host (Alq_3 or BP4mPy) doped with *x* wt. % **5** (30 nm)/ETL (Alq_3 or BP4mPy) (40 nm)/ LiF (0.5 nm)/Al (150 nm). In general, the concentrations of all RGB dopants in phosphorescent OLEDs range from 6 to 10 wt.%. However, NIR OLEDs usually require higher concentrations to achieve the desired red-shifted EL spectrum; therefore, 8 wt.% and 16 wt.% concentrations were used here. The EL spectrum from the device with 16 wt.% of dopant was slightly red-shifted compared to the EL spectrum from the device with 8 wt.% of dopant. However, the device adopting 8 wt.% doping concentration achieved a much higher efficiency value. Consequently, the doping concentration at 8 wt.% was used in this study. Furthermore, based on our experience, the device efficiency can be improved by using a second dopant with an intermediate energy level to provide a favorable stepwise energy transfer. The Os(II) complex $[\text{Os}(\text{fptz})_2(\text{PPh}_2\text{Me})_2]$ (**7**) was selected for this purpose as it exhibited considerable spectral overlap with that of **5**, as well as the optimal energy levels.^{40, 67-69} This isoenergetic relationship allows efficient energy transfer from **7** to **5**, and the emission remained unaltered, due to the low concentration of **7**.^{38, 64} Therefore, the doped devices A2 and B2 were represented by the architectures: ITO/ NPB (40

nm)/Host (Alq₃ or BP4mPy) doped with 8 wt.% **5** and 0.1 wt.% **7** (30 nm)/ETL (Alq₃ or BP4mPy) (40 nm)/ LiF (0.5 nm)/Al (150 nm). The materials employed in OLEDs along with complex **5** and an estimated energy-level diagram for the devices are depicted in Figure 5.

The characteristics of the resulting devices are shown in Figure 6, while the numerical data are listed in Table 5. As can be seen, all devices show nearly identical spectral profiles, for which the EL peak maxima (690 nm) show broadened full width at half maximum (FWHM) of approx. 130 nm (or 2680 cm⁻¹) and are also slightly blue-shifted with respect to the photoluminescence (PL) recorded as neat powder (717 nm). It appears to us that, the blue-shifting in EL spectra may be due to the effect of media, for which the co-deposition in host material may somewhat destabilize the ³MLCT excited states. Furthermore, the lack of Alq₃ or BP4mPy emissions implies that complete energy transfers take place from the hosts to the NIR dopant **5**. Hence, the carrier recombination zone was confined within the emitting layer and the exciton diffusion to the adjacent carrier transport layers are avoided in the devices.

Moreover, the respective turn-on voltages (defined as a sharp rise in current density) for devices A1, A2, B1, and B2 are found to be 2.2 V, 2.2 V, 3.0 V and 3.0 V, respectively. Obviously, the higher band gap of BP4mPy produced higher operation voltages and lower current densities for devices B1 and B2 versus devices A1 and A2 that were fabricated using Alq₃. As shown in Figures 6(c) and (d), devices A1 and A2 showed poor external quantum efficiencies (EQE) at lower current densities, which might be attributed to the quenching induced by the charge carrier-exciton interaction.⁷⁰ Peak EQEs of A1 and A2 were recorded to be 1.54% (0.17 lm/W) and 1.56% (0.18 lm/W), respectively. In contrast, the peak EQEs of B1 and B2 were higher,

e.g. 2.27% (0.13 lm/W) and 2.13% (0.17 lm/W), respectively. This approx. 47% increase in EQEs demonstrated the effectiveness of BP4mPy in achieving the balanced carrier transport. On the other hand, both the co-doped devices A2 and B2 showed improved carrier transporting ability and, hence, increased max. power efficiency as compared to those without the co-dopant **7** (i.e. A1 and B1).

In addition, the EQEs of devices A1 and A2 (i.e. with Alq₃) decreased to one-half of their highest values at a current density ($J_{1/2}$) of 473.2 and 441.9 mA/cm², and at $J_{1/2}$ of 82.3 and 69.5 mA/cm² for B1 and B2 (i.e. BP4mPy).^{71, 72} Devices A1 and A2 showed much higher overall current densities because of the reduced efficiency roll-off, which is partially attributed to the lower electron mobility of Alq₃ (~10⁻⁵ cm²/Vs). Therefore, the relatively faster hole injection from NPB to Alq₃ enlarged the recombination zone (RZ) and thus decreased the exciton concentration. In contrast, BP4mPy with a higher electron mobility of ~10⁻⁴ cm²/Vs restrained the thickness of RZ, resulting in a relatively higher exciton concentration in a narrow space. The increase in triplet excitons with long excited-state lifetimes would substantially increase the probability of triplet-triplet annihilation as well as triplet polaron quenching.⁷³⁻⁷⁵ As such, devices B1 and B2 only achieved light output of 48.9 and 45.9 mW/cm² at 16.0 V and 15.8 V. In contrast, forward light output as high as 53.9 and 93.26 mW/cm² can be reached at lower voltages of 11.4 V and 11.0 V for devices A1 and A2, respectively.

Conclusion

In summary, a new series of NIR-emitting Os(II) phosphors bearing heteroleptic *tris*-bidentate chelating architecture were synthesized and characterized, among which the Os(II) complexes **5** and **6** showed PL emission at 717 nm with $\Phi = 8.8\%$ and at 779 nm with $\Phi = 4.5\%$, respectively in the solid state. Their lower-energy emissions are generally derived from the mixed ³MLCT and ³LLCT excited states, while the higher emission efficiencies are, in part, attributed to the higher rigidity of

coordinated phenanthroline that reduced the vibronic coupling in the excited states. Hence, a better emission efficiency than predicted by energy gap law can be achieved.

NIR-emitting OLEDs were fabricated using the highly emissive Os(II) phosphor **5**, giving a peak external quantum efficiency (EQE) of 1.54%, a power efficiency (PE) of 0.17 lm/W, and a low turn-on voltage of 2.2 V with Alq₃ as both host and ETL. In addition, the peak EQE increased to 2.27% by substituting Alq₃ with BP4mPy, due to the better carrier balance and exciton confinement. Overall, these results pinpoint the great potential of the relevant Os(II) phosphors in the fabrication of NIR-emitting OLEDs.

Experimental Section:

General Information and Materials. Mass spectra were measured on a JEOL SX-102A instrument operating in electron impact (EI) mode or fast atom bombardment (FAB) mode. ¹H, ¹⁹F and ³¹P NMR spectra were obtained using the Varian Mercury-400 or INOVA-500 instruments. Elemental analyses were performed using the NSC Regional Instrumentation Center at National Chao Tung University, Hsinchu, Taiwan. 5,5'-Di(trifluoromethyl)-2H,2'H-3,3'-bipyrazole (bipzH₂) was prepared according to literature procedure.⁷⁶ All reactions were carried out under N₂ atmosphere and anhydrous conditions.

Photophysical measurement. Steady-state absorption and emission spectra were recorded by a Hitachi (U-3310) spectrophotometer and an Edinburgh (FS920) fluorimeter, respectively. The Q.Y. of the titled complexes in solid was measured by an integrating sphere,^{77, 78} which has been calibrated by wavelength response and incorporated into the aforementioned fluorimeter, to obtain the absolute emission yield.

Cyclic voltammetry. All electrochemical potentials were measured in a 0.1 M TBAPF₆/CH₂Cl₂ and THF solution for oxidation and reduction reaction, and reported in volts using FcH/FcH⁺ as reference; ΔE_p is defined as E_{ap} (anodic peak potential) – E_{cp} (cathodic peak potential) and these data are quoted in mV. The Pt electrode and Au(Hg) alloy were selected as the working electrode of oxidation and reduction processes, respectively.

Preparation of 1b. A mixture of Os₃(CO)₁₂ (100 mg, 0.11 mmol), bipzH₂ (93 mg, 0.34 mmol) and bipyridine (bpy, 53 mg, 0.340 mmol) in diethylene glycol monomethyl ether (DGME, 10 mL) was heated to 190°C for 24 hr. After cooling to RT, the solvent was removed under vacuum. The residue was purified by silica gel column chromatography eluting with EA: hexane (2: 1), followed by recrystallization from a mixture of EA and hexane, giving yellow solid (**1b**, 141 mg, 0.21 mmol, 63%).

Spectroscopic data of 1b: ¹H NMR (400 MHz, d₆-acetone, 294K): δ 9.47 (dd, J = 5.6, 0.8 Hz, 1H), 8.76 (d, J = 8.4 Hz, 1H), 8.69 (d, J = 8.4 Hz, 1H), 8.45 (td, J = 8.0, 0.8 Hz, 1H), 8.29 (td, J = 8.0, 0.8 Hz, 1H), 7.88 (td, J = 6.8, 0.8 Hz, 1H), 7.68 (td, J = 6.8, 0.8 Hz, 1H), 7.37 (d, J = 6.8 Hz, 1H), 6.70 (s, 1H), 6.48 (s, 1H); ¹⁹F-¹H NMR (470 MHz, d₆-acetone, 294K): δ -60.62 (s, 3F), -60.84 (s, 3F); MS (FAB, ¹⁹²Os): m/z 672 (M-2)⁺, 645 (M⁺-CO), 616(M⁺-2CO); IR (CH₂Cl₂): ν (CO), 1978 (s), 2040 (s) cm⁻¹; Anal. Calcd. for C₂₀H₁₀F₆N₆O₂Os: N, 12.53; C, 35.82; H, 1.50. Found: N, 12.17; C, 35.62; H, 1.94.

Selected crystal data of 1b: C₄₄H₂₈F₁₂N₁₂O₆Os₂; M = 1429.18; triclinic; space group = *P*-1; a = 10.1401(7) Å, b = 14.5567(10) Å, c = 17.5318(12) Å, α = 82.8000(14)°, β = 79.8955(15)°, γ = 83.7633(15)°, V = 2517.6(3) Å³; Z = 2; ρ_{calcd} = 1.885 Mg·m⁻³; $F(000)$ = 1368; crystal size = 0.40 × 0.40 × 0.25 mm³; λ (Mo-K α) = 0.71073 Å; T = 150(2) K; μ = 5.145 mm⁻¹; 29504 reflections collected, 11522 independent reflections (R_{int} = 0.0358), GOF = 1.061, final $R_1[I > 2\sigma(I)]$ = 0.0353 and $wR_2(\text{all data})$ = 0.1026.

Preparation of 3. A mixture of Os₃(CO)₁₂ (100 mg, 0.11 mmol), bipzH₂ (93 mg, 0.34 mmol) and bpy (53 mg, 0.34 mmol) in 10 mL DGME was heated to 190°C for 24 hr. After the reaction mixture was cooled to RT, freshly sublimed Me₃NO (52 mg, 0.69

mmol) was added and the solution was then heated to 110°C for 1 hr. After then, 1,2-bis(phospholano)benzene (pp2b, 91 mg, 0.36 mmol) was added into the solution and then heated to 190°C for 12 hr. Finally, the solvent was removed under vacuum, and the residue was purified by silica gel column chromatography eluting with EA: hexane (2: 1). Recrystallization from a mixture of EA and hexane gave dark-brown crystalline solid (90 mg, 0.10 mmol, 31%).

Spectroscopic data of 3: ^1H NMR (400 MHz, d_6 -acetone, 294K): δ 8.65 (d, $J = 5.6$ Hz, 1H), 8.41 (d, $J = 8.0$ Hz, 2H), 7.87 (m, 3H), 7.79 (m, 2H), 7.50 (m, 2H), 7.37 (t, $J = 6.4$ Hz, 1H), 7.17 (t, $J = 6.4$ Hz, 1H), 6.54 (s, 1H), 6.39 (s, 1H), 3.61 (m, 1H), 2.62 (m, 1H), 2.47 (m, 1H), 2.15 (m, 1H), 1.80 (m, 3H), 1.68 (m, 1H), 1.27 (m, 5H), 0.77 (m, 3H); ^{19}F - $\{^1\text{H}\}$ NMR (470 MHz, d_6 -acetone, 294K): δ -59.62 (s, 3F), -59.65 (s, 3F); ^{31}P NMR (202 MHz, d_6 -acetone, 298K): δ 39.88 (s, 1P), δ 33.80 (s, 1P). MS (FAB, ^{192}Os): m/z 866 (M^+); Anal. Calcd. for $\text{C}_{32}\text{H}_{30}\text{F}_6\text{N}_6\text{OsP}_2$: N, 9.72; C, 44.44; H, 3.50. Found: N, 9.36; C, 43.99; H, 3.76.

Selected crystal data of 3: $\text{C}_{35}\text{H}_{37}\text{F}_6\text{N}_6\text{OsP}_2$; $M = 907.85$; monoclinic; space group = $C2/c$; $a = 23.1156(7)$ Å, $b = 16.4313(5)$ Å, $c = 18.4153(5)$ Å, $\beta = 96.193(2)^\circ$, $V = 6953.7(4)$ Å 3 ; $Z = 8$; $\rho_{\text{calcd}} = 1.734$ Mg·m $^{-3}$; $F(000) = 3592$; crystal size = $0.20 \times 0.15 \times 0.03$ mm 3 ; $\lambda(\text{Mo-K}\alpha) = 0.71073$ Å; $T = 150(2)$ K; $\mu = 3.828$ mm $^{-1}$; 23283 reflections collected, 7950 independent reflections ($R_{\text{int}} = 0.0554$), GOF = 1.056, final $R_1[I > 2\sigma(I)] = 0.0482$ and $wR_2(\text{all data}) = 0.1409$.

Preparation of 4. Similar to the procedure described for **3**, this reaction was conducted using $\text{Os}_3(\text{CO})_{12}$ (100 mg, 0.11 mmol), bipzH $_2$ (93 mg, 0.34 mmol), 1,10-phenanthroline (61 mg, 0.34 mmol), and then Me $_3$ NO (52 mg, 0.69 mmol) and pp2b (91 mg, 0.36 mmol), giving dark-brown crystalline solid (105 mg, 0.12 mmol) in 35% yield.

Spectroscopic data of 4: ^1H NMR (400 MHz, d_6 -acetone, 294K): δ 9.09 (d, $J = 5.2$ Hz, 1H), 8.44 (m, 2H), 8.04 (m, 3H), 7.93 (t, $J = 7.2$ Hz, 1H), 7.76 (m, 2H), 7.52 (m, 3H), 6.59 (s, 1H), 6.38 (s, 1H), 3.71 (m, 1H), 2.67 (m, 2H), 2.14 (m, 1H), 1.90 (m, 2H), 1.63

(m, 2H), 1.20 (m, 4H), 0.82 (m, 3H), 0.21 (m, 1H); ^{19}F - $\{^1\text{H}\}$ NMR (470 MHz, d_6 -acetone, 294K): δ -59.51 (s, 3F), -59.69 (s, 3F); ^{31}P NMR (202 MHz, d_6 -acetone, 298K): δ 39.13 (s, 1P), 33.53 (s, 1P). MS (FAB, ^{192}Os): m/z 890 (M^+); Anal. Calcd. for $\text{C}_{34}\text{H}_{30}\text{F}_6\text{N}_6\text{OsP}_2$: N, 9.46; C, 45.94; H, 3.40. Found: N, 9.23; C, 45.98; H, 3.95.

Preparations of 5 and 6. The Os(II) complexes **5** and **6** were obtained in 21% and 27% yields respectively using similar procedures as described for preparation for **4**.

Spectroscopic data of 5: ^1H NMR (400 MHz, d_6 -acetone, 294K): δ 8.83 (s, 1H), 8.21 (q, $J = 9.6$ Hz, 2H), 7.91 (t, $J = 6.8$ Hz, 1H), 7.74 (t, $J = 6.8$ Hz, 1H), 7.64 (d, $J = 2.8$ Hz, 2H), 7.44 (m, 2H), 6.57 (s, 1H), 6.38 (s, 1H), 3.73 ~ 3.65 (m, 1H), 2.73 ~ 2.63 (m, 8H), 2.39 (s, 3H), 2.31 (s, 3H), 2.18 ~ 2.11 (m, 1H), 1.96 ~ 1.82 (m, 2H), 1.73 ~ 1.63 (m, 3H), 1.28 ~ 1.13 (m, 3H), 1.03 ~ 0.93 (m, 1H), 0.86 ~ 0.75 (m, 2H), 0.27 ~ 0.20 (m, 1H); ^{19}F - $\{^1\text{H}\}$ NMR (470 MHz, d_6 -acetone, 294K): δ -59.42 (s, 3F), -59.68 (s, 3F); ^{31}P NMR (202 MHz, d_6 -acetone, 298K): δ 38.81 (s, 1P), 33.74 (s, 1P). MS (FAB, ^{192}Os): m/z 946 (M^+); Anal. Calcd. for $\text{C}_{38}\text{H}_{38}\text{F}_6\text{N}_6\text{OsP}_2$: N, 8.89; C, 48.30; H, 4.05. Found: N, 9.12; C, 48.37; H, 4.28.

Spectroscopic data of 6: ^1H NMR (400 MHz, d_6 -acetone, 294K): δ 9.19 (d, $J = 5.6$ Hz, 1H), 8.17 ~ 8.08 (m, 3H), 7.95 (t, $J = 6.8$ Hz, 1H), 7.80 ~ 7.76 (m, 2H), 7.70 ~ 7.52 (m, 13H), 6.61 (s, 1H), 6.42 (s, 1H), 3.81 ~ 3.74 (m, 1H), 2.74 ~ 2.70 (m, 2H), 2.23 ~ 2.12 (m, 1H), 1.99 ~ 1.86 (m, 1H), 1.77 ~ 1.51 (m, 3H), 1.36 ~ 1.14 (m, 4H), 0.97 ~ 0.77 (m, 3H), 0.46 ~ 0.32 (m, 1H); ^{19}F - $\{^1\text{H}\}$ NMR (470 MHz, d_6 -acetone, 294K): δ -59.59 (s, 3F), -59.61 (s, 3F); ^{31}P NMR (202 MHz, d_6 -acetone, 298K): δ 38.93 (s, 1P), 33.89 (s, 1P). MS (FAB, ^{192}Os): m/z 1042 (M^+); Anal. Calcd. for $\text{C}_{46}\text{H}_{38}\text{F}_6\text{N}_6\text{OsP}_2$: N, 8.07; C, 53.07; H, 3.68. Found: N, 7.99; C, 52.58; H, 3.90.

Single Crystal X-Ray Diffraction Studies. Single crystal X-ray diffraction studies were measured on a Bruker SMART Apex CCD diffractometer using (Mo-K_α) radiation ($\lambda = 0.71073$ Å). The data collection was executed using the SMART program. Cell refinement and data reduction were performed with the SAINT program. The

structure was determined using the SHELXTL/PC program and refined using full-matrix least squares. CCDC 1044312 and 1044313 contain the supplementary crystallographic data for this paper. These data can be obtained free of charge from the Cambridge Crystallographic Data Centre via www.ccdc.cam.ac.uk/data_request/cif.

Computational Methods. All the calculations were performed with the Gaussian 09 program package, using the B3LYP functional,^{79, 80} LANL2DZ⁸¹ basis set for Os and 6-31G**⁸² for all other atoms. A conductor-like polarization continuum model CPCM of CH₂Cl₂ solvent was applied to all calculations, and results analyzed further with GaussSum.⁸³ Structures obtained were confirmed as true minima by the absence of imaginary frequencies.

OLED Fabrication. All commercial materials and ITO-coated glass were purchased from Nichem and Lumtec. Before thermal evaporation, materials were subjected to temperature-gradient sublimation under high vacuum ($\sim 10^{-6}$ torr). The bottom-emitting OLED architecture consists of multiple organic layers and a reflective cathode which were consecutively deposited onto the ITO-coated glass substrate. The deposition rates of organics and aluminum were kept at ~ 0.1 nm/s and 0.5 nm/s, respectively. The active area was defined by the shadow mask (2×2 mm²). The measurement of EL characteristics was conducted in a glove box filled with nitrogen. Current density-voltage-luminance characterization was measured using a Keithley 238 current source-measure unit and a Keithley 6485 picoammeter equipped with a calibrated Si-photodiode. The electroluminescent spectra were recorded using an Ocean Optics spectrometer.

Acknowledgments. This work was supported by the Ministry of Science and Technology of Taiwan, under the grant number 101-2113-M-007-013-MY3 and 102-2221-E-155-080-MY3. P.J.L. gratefully acknowledges support from the Australian Research Council and the award of a Future Fellowship [FT120100073].

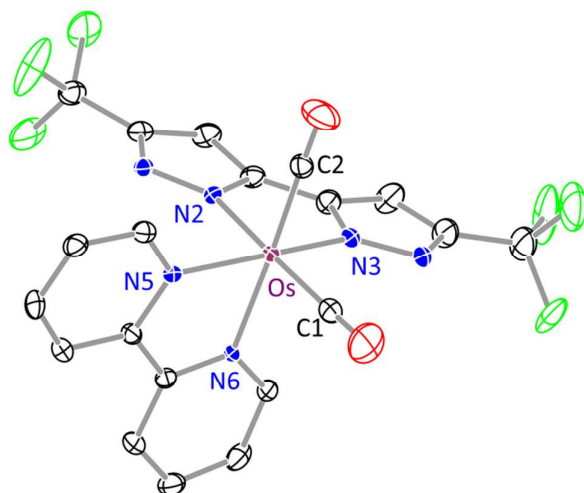


Figure 1. ORTEP diagram of **1b** with thermal ellipsoids shown at 30% probability level; selected bond distances: Os-N(2) = 2.102(4), Os-N(3) = 2.057(4), Os-N(5) = 2.080(4), Os-N(6) = 2.121(4), Os-C(1) = 1.892(6) and Os-C(2) = 1.895(6) Å; bond angles: \angle C(1)-Os-C(2) = 87.8(2), N(5)-Os-N(6) = 77.94(16) and N(2)-Os-N(3) = 76.85 (17)°.

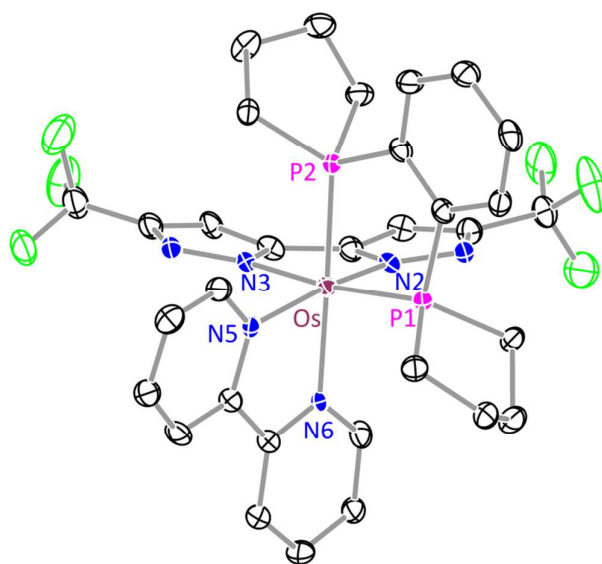


Figure 2. ORTEP diagram of **3** with thermal ellipsoids shown at 30% probability level; selected bond distances: Os-N(2) = 2.088(5), Os-N(3) = 2.113(6), Os-N(5) = 2.072(6), Os-N(6) = 2.123(5), Os-P(1) = 2.2650(17) and Os-P(2) = 2.2618(17) Å; bond angles: \angle P(1)-Os-P(2) = 85.36(6), N(5)-Os-N(6) = 77.1(2) and N(2)-Os-N(3) = 76.2(2)°.

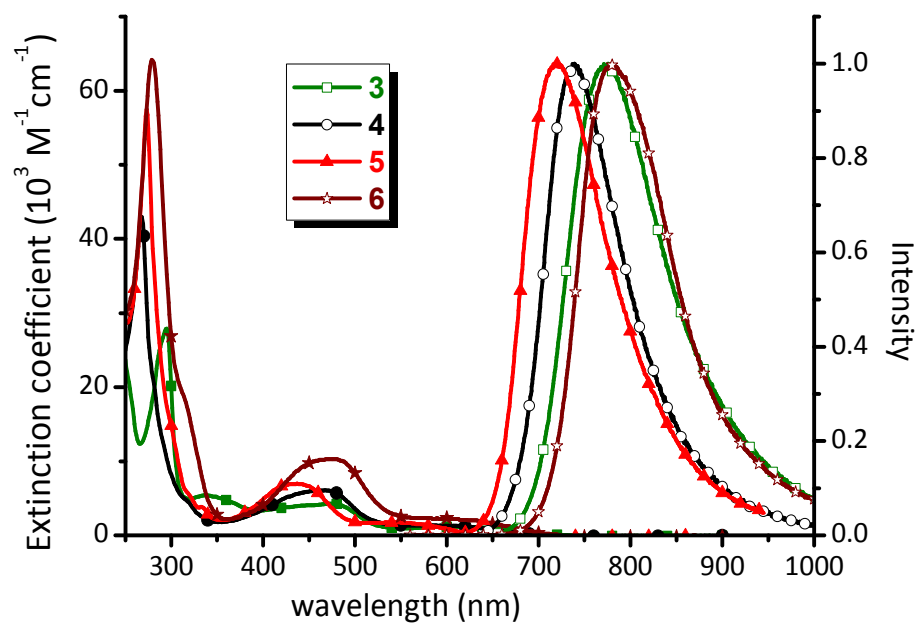


Figure 3. UV-Vis absorption spectra in CH₂Cl₂ and solid state emission spectra at RT of Os(II) complexes **3** – **6**.

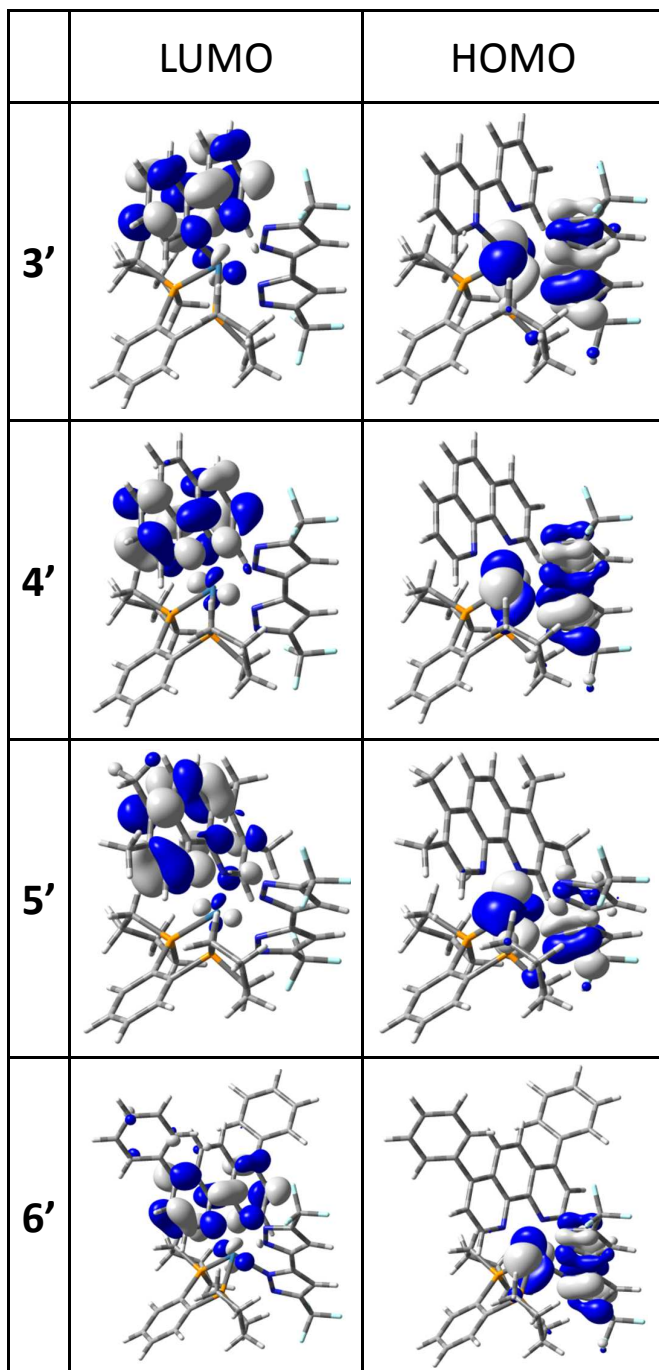


Figure 4. Frontier molecular orbitals in the lowest-energy optical transitions for Os(II) complexes **3'** – **6'**; all contours are plotted at ± 0.04 (e/bohr^3)^{1/2}.

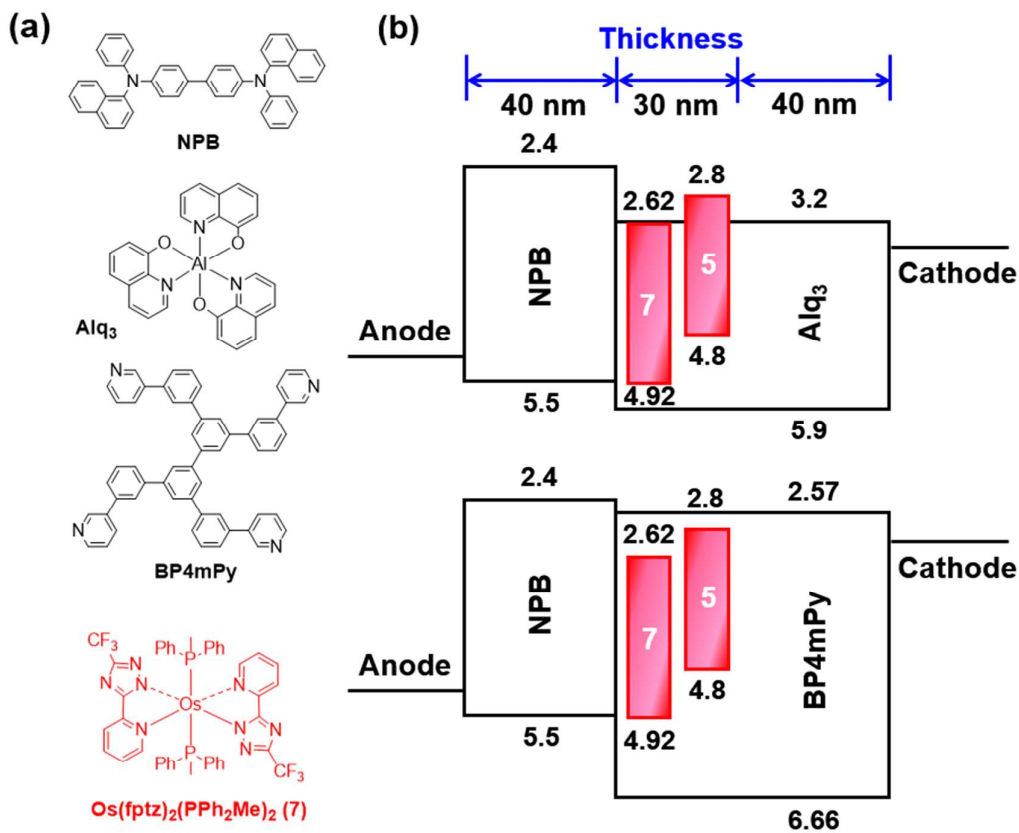


Figure 5. (a) Compounds used in OLEDs along with complex 5; (b) architectures of NIR OLEDs with the tested hosts, dopants and electron transport layers.

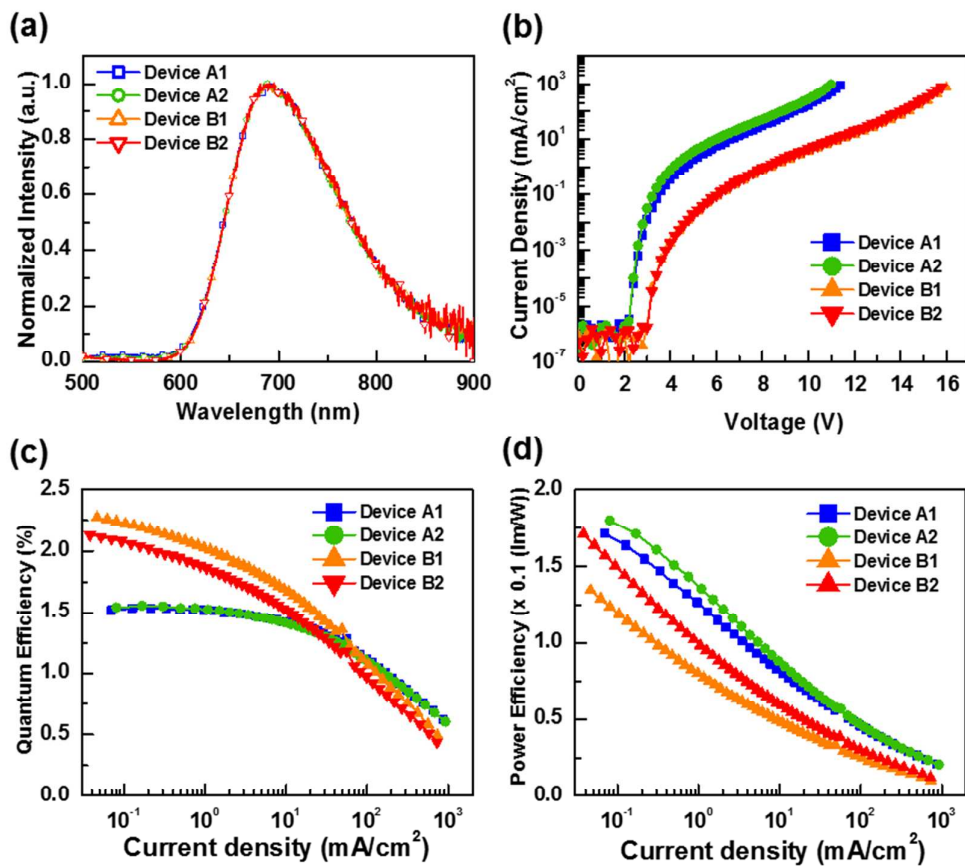


Figure 6. (a) EL spectra of tested OLEDs; (b) current density-voltage-luminance (J - V - L) plots; (c) external quantum efficiency vs. current density; (d) power efficiency vs. current density for devices A1, A2, B1 and B2.

Table 1. Photophysical properties for the NIR-emitting Os(II) complexes **3** – **6**.

	abs. λ_{\max} (nm) [ϵ ($10^3 \text{ M}^{-1}\text{cm}^{-1}$)] ^a	PL λ_{\max} (nm) ^b	Φ (%) ^b	τ_{obs} (ns) ^b	k_r (10^5 s^{-1})	k_{nr} (10^7 s^{-1})
3	295 [27.9], 338 [5.4], 471 [4.1], 610 [1.2]	772	0.5	26.4	1.89	3.76
4	268 [43.0], 406 [6.1], 586 [1.2]	739	3.1	197	1.52	0.49
5	273 [57.4], 442 [6.9], 545 [1.7]	717	8.8	431	2.04	0.21
6	279 [64.2], 476 [10.3], 599 [2.1]	779	4.5	115	3.91	0.83

^a UV-Vis spectra were recorded in 10^{-5} M in CH_2Cl_2 solution. ^b Photoluminescence spectra and quantum yields were measured as neat powder.

Table 2. Electrochemical properties for the studied Os(II) complexes.

	ox. $E_{1/2}$ V^a [ΔE_p (mV)]	red. $E_{1/2}$ V^b [ΔE_p (mV)]		HOMO eV ^c	LUMO eV ^c
3	0.07 [89]	-2.14 [124]	3'	-5.00	-2.16
4	0.07 [99]	-2.22 [83]	4'	-5.00	-2.13
5	0.00 [88]	-2.30 [73]	5'	-5.03	-1.91
6	0.07 [72]	-2.04 [73]	6'	-4.98	-2.18

^a Measured in 0.1 M TBAPF₆/CH₂Cl₂ vs FcH⁺/FcH with Pt working electrode.

^b Measured in 0.1 M TBAPF₆/THF vs FcH⁺/FcH with Au working electrode.

^c B3LYP/LANL2DZ:6-31G** data.

Table 3. Selected bond lengths (Å) and angles (°) from **3** and the computational models **3'**, **4'**, **5'** and **6'**.

	3	3'	4'	5'	6'
Os-N(2) (in Å)	2.088(5)	2.1101	2.1077	2.0898	2.1098
Os-N(3)	2.113(6)	2.1346	2.1349	2.1041	2.1353
Os-N(5)	2.072(6)	2.1094	2.1207	2.0909	2.1192
Os-N(6)	2.123(5)	2.1276	2.1387	2.1149	2.1308
Os-P(1)	2.2650(17)	2.3334	2.3312	2.3068	2.3337
Os-P(2)	2.2618(17)	2.3204	2.3174	2.3013	2.3185
P(1)-Os-P(2) (in °)	85.36(6)	84.48	84.63	85.38	84.49
N(2)-Os-N(3)	76.2(2)	75.95	76.05	75.92	75.94
N(5)-Os-N(6)	77.1(2)	76.92	77.71	77.96	77.26

Table 4. Calculated $S_0 \rightarrow S_1$ and $S_0 \rightarrow T_1$ transition energies (in nm), orbital analysis and optical properties of **3'**, **4'**, **5'** and **6'**.

	$S_0 \rightarrow S_1$	$S_0 \rightarrow T_1$	λ_{\max} (abs)	λ_{\max} (em)
3'	HOMO \rightarrow LUMO (95%)	HOMO \rightarrow LUMO (76%)	610	772
4'	HOMO \rightarrow LUMO (95%)	HOMO \rightarrow LUMO (70%)	586	739
5'	HOMO \rightarrow LUMO (58%) HOMO \rightarrow LUMO+1 (33%)	HOMO-1 \rightarrow LUMO (52%) HOMO-2 \rightarrow LUMO (26%)	545	717
6'	HOMO \rightarrow LUMO (93%)	HOMO \rightarrow LUMO (63%)	599	779

Table 5. EL Characteristics of NIR OLEDs with Different Dopants.

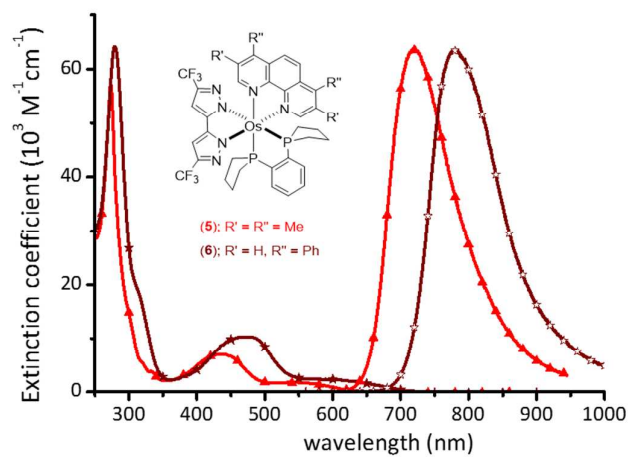
Device		A1	A2	B1	B2
Host & ETL		<i>Alq₃</i>		<i>BP4mPy</i>	
Dopant		5	5 + Os	5	5 + Os
External Quantum Efficiency (%)	max.	1.54	1.56	2.27	2.13
	10 mA/cm ²	1.42	1.41	1.68	1.53
Power Efficiency (lm/W)	max.	0.17	0.18	0.13	0.17
	10 mA/cm ²	0.08	0.09	0.05	0.06
turn on voltage (V)		2.2	2.2	3.0	3.0
$J_{1/2}$ (mA/cm ²)		473.2	441.9	82.3	69.5
CIE 1931 coordinates		(0.66, 0.34)	(0.67, 0.33)	(0.69, 0.31)	(0.69, 0.31)
Light output (mW/cm ²) [@V]		53.9 [11.4 V]	52.8 [11.0 V]	48.9 [16.0 V]	45.9 [15.8 V]

1. R. C. Evans, P. Douglas and C. J. Winscom, *Coord. Chem. Rev.*, 2006, **250**, 2093.
2. P.-T. Chou and Y. Chi, *Chem. Eur. J.*, 2007, **13**, 380.
3. J. A. G. Williams, S. Develay, D. L. Rochester and L. Murphy, *Coord. Chem. Rev.*, 2008, **252**, 2596.
4. A. F. Rausch, M. E. Thompson and H. Yersin, *J. Phys. Chem. A*, 2009, **113**, 5927.
5. A. F. Rausch, H. H. H. Homeier and H. Yersin, *Top. Organomet. Chem.*, 2010, **29**, 193.
6. Y. Chi and P.-T. Chou, *Chem. Soc. Rev.*, 2010, **39**, 638.
7. P.-T. Chou, Y. Chi, M.-W. Chung and C.-C. Lin, *Coord. Chem. Rev.*, 2011, **255**, 2653.
8. J. Kalinowski, V. Fattori, M. Cocchi and J. A. G. Williams, *Coord. Chem. Rev.*, 2011, **255**, 2401.
9. Y. Chi, B. Tong and P.-T. Chou, *Coord. Chem. Rev.*, 2014, **281**, 1-25.
10. Y. You and S. Y. Park, *Dalton Trans.*, 2009, 1267.
11. G. Zhou, W.-Y. Wong and S. Suo, *J. Photochem. Photobiol. C*, 2010, **11**, 133.
12. L. Xiao, Z. Chen, B. Qu, J. Luo, S. Kong, Q. Gong and J. Kido, *Adv. Mater.*, 2011, **23**, 926.
13. H. Sasabe and J. Kido, *Eur. J. Org. Chem.*, 2013, **2013**, 7653-7663.
14. B. D'Andrade, *Nat. Photon.*, 2007, **1**, 33.
15. K. T. Kamtekar, A. P. Monkman and M. R. Bryce, *Adv. Mater.*, 2010, **22**, 572.
16. M. C. Gather, A. Koehnen and K. Meerholz, *Adv. Mater.*, 2011, **23**, 233.
17. H. Sasabe and J. Kido, *J. Mater. Chem. C*, 2013, **1**, 1699.
18. Y.-L. Chang and Z.-H. Lu, *J. Display Tech.*, 2013, **9**, 459-468.
19. J. Chen, F. Zhao and D. Ma, *Mater. Today*, 2014, **17**, 175-183.
20. W. Kaim, *Coord. Chem. Rev.*, 2011, **255**, 2503.
21. V. J. Pansare, S. Hejazi, W. J. Faenza and R. K. Prud'homme, *Chem. Mater.*, 2012, **24**, 812-827.
22. H. Xiang, J. Cheng, X. Ma, X. Zhou and J. J. Chruma, *Chem. Soc. Rev.*, 2013, **42**, 6128-6185.
23. M. A. Bennett, S. K. Bhargava, E. C.-C. Cheng, W. H. Lam, T. K.-M. Lee, S. H. Priver, J. Wagler, A. C. Willis and V. W.-W. Yam, *J. Am. Chem. Soc.*, 2010, **132**, 7094.
24. E. Rossi, L. Murphy, P. L. Brothwood, A. Colombo, C. Dragonetti, D. Roberto, R. Ugo, M. Cocchi and J. A. G. Williams, *J. Mater. Chem.*, 2011, **21**, 15501-15510.
25. M.-H. Nguyen and J. H. K. Yip, *Organometallics*, 2011, **30**, 6383-6392.
26. X. Wu, Y. Liu, Y. Wang, L. Wang, H. Tan, M. Zhu, W. Zhu and Y. Cao, *Org. Electron.*, 2012, **13**, 932-937.
27. Y. Zems, A. G. Moiseev and D. F. Perepichka, *Org. Lett.*, 2013, **15**, 5330-5333.

28. Y. Sun, C. Borek, K. Hanson, P. I. Djurovich, M. E. Thompson, J. Brooks, J. J. Brown and S. R. Forrest, *Appl. Phys. Lett.*, 2007, **90**, 213503.
29. K. R. Graham, Y. Yang, J. R. Sommer, A. H. Shelton, K. S. Schanze, J. Xue and J. R. Reynolds, *Chem. Mater.*, 2011, **23**, 5305.
30. A. Damas, M. P. Gullo, M. N. Rager, A. Jutand, A. Barbieri and H. Amouri, *Chem. Commun.*, 2013, **49**, 3796-3798.
31. E. L. Williams, J. Li and G. E. Jabbour, *Appl. Phys. Lett.*, 2006, **89**, 083506.
32. H.-Y. Chen, C.-H. Yang, Y. Chi, Y.-M. Cheng, Y.-S. Yeh, P.-T. Chou, H.-Y. Hsieh, C.-S. Liu, S.-M. Peng and G.-H. Lee, *Can. J. Chem.*, 2006, **84**, 309.
33. R. Tao, J. Qiao, G. Zhang, L. Duan, L. Wang and Y. Qiu, *J. Phys. Chem. C*, 2012, **116**, 11658.
34. X. Cao, J. Miao, M. Zhu, C. Zhong, C. Yang, H. Wu, J. Qin and Y. Cao, *Chem. Mater.*, 2015, **27**, 96-104.
35. M. Schulze, A. Steffen and F. Würthner, *Angew. Chem. Int. Ed.*, 2015, DOI: 10.1002/anie.201410437.
36. T.-C. Lee, J.-Y. Hung, Y. Chi, Y.-M. Cheng, G.-H. Lee, P.-T. Chou, C.-C. Chen, C.-H. Chang and C.-C. Wu, *Adv. Funct. Mater.*, 2009, **19**, 2639.
37. B.-S. Du, J.-L. Liao, M.-H. Huang, C.-H. Lin, H.-W. Lin, Y. Chi, H.-A. Pan, G.-L. Fan, K.-T. Wong, G.-H. Lee and P.-T. Chou, *Adv. Funct. Mater.*, 2012, **22**, 3491.
38. J.-L. Liao, Y. Chi, S.-H. Liu, G.-H. Lee, P.-T. Chou, H.-X. Huang, Y.-D. Su, C.-H. Chang, J.-S. Lin and M.-R. Tseng, *Inorg. Chem.*, 2014, **53**, 9366-9374.
39. P.-C. Wu, J.-K. Yu, Y.-H. Song, Y. Chi, P.-T. Chou, S.-M. Peng and G.-H. Lee, *Organometallics*, 2003, **22**, 4938-4946.
40. Y.-L. Tung, P.-C. Wu, C.-S. Liu, Y. Chi, J.-K. Yu, Y.-H. Hu, P.-T. Chou, S.-M. Peng, G.-H. Lee, Y. Tao, A. J. Carty, C.-F. Shu and F.-I. Wu, *Organometallics*, 2004, **23**, 3745.
41. F.-C. Hsu, Y.-L. Tung, Y. Chi, C.-C. Hsu, Y.-M. Cheng, M.-L. Ho, P.-T. Chou, S.-M. Peng and A. J. Carty, *Inorg. Chem.*, 2006, **45**, 10188-10196.
42. S.-H. Chang, C.-F. Chang, J.-L. Liao, Y. Chi, D.-Y. Zhou, L.-S. Liao, T.-Y. Jiang, T.-P. Chou, E. Y. Li, G.-H. Lee, T.-Y. Kuo and P.-T. Chou, *Inorg. Chem.*, 2013, **52**, 5867.
43. J.-L. Liao, Y. Chi, Y.-D. Su, H.-X. Huang, C.-H. Chang, S.-H. Liu, G.-H. Lee and P.-T. Chou, *J. Mater. Chem. C*, 2014, **2**, 6269-6282.
44. Y.-M. Cheng, G.-H. Lee, P.-T. Chou, L.-S. Chen, Y. Chi, C.-H. Yang, Y.-H. Song, S.-Y. Chang, P.-I. Shih and C.-F. Shu, *Adv. Funct. Mater.*, 2008, **18**, 183.
45. S. Joerg, R. S. Drago and J. Sales, *Organometallics*, 1998, **17**, 589.
46. S.-W. Li, Y.-M. Cheng, Y.-S. Yeh, C.-C. Hsu, P.-T. Chou, S.-M. Peng, G.-H. Lee, Y.-L. Tung, P.-C. Wu, Y. Chi, F.-I. Wu and C.-F. Shu, *Chem. Eur. J.*, 2005, **11**, 6347.
47. L.-M. Huang, G.-M. Tu, Y. Chi, W.-Y. Hung, Y.-C. Song, M.-R. Tseng, P.-T. Chou,

- G.-H. Lee, K.-T. Wong, S.-H. Cheng and W.-S. Tsai, *J. Mater. Chem. C*, 2013, **1**, 7582-7592.
48. H.-Y. Ku, B. Tong, Y. Chi, H.-C. Kao, C.-C. Yeh, C.-H. Chang and G.-H. Lee, *Dalton Trans.*, 2015, DOI: 10.1039/C1034DT03028A.
49. E. M. Kober, J. L. Marshall, W. J. Dressick, B. P. Sullivan, J. V. Caspar and T. J. Meyer, *Inorg. Chem.*, 1985, **24**, 2755-2763.
50. E. M. Kober, J. V. Caspar, R. S. Lumpkin and T. J. Meyer, *J. Phys. Chem.*, 1986, **90**, 3722-3734.
51. M. V. Werrett, D. Chartrand, J. D. Gale, G. S. Hanan, J. G. MacLellan, M. Massi, S. Muzzioli, P. Raiteri, B. W. Skelton, M. Silberstein and S. Stagni, *Inorg. Chem.*, 2011, **50**, 1229-1241.
52. K. P. S. Zanoni, B. K. Kariyazaki, A. Ito, M. K. Brennaman, T. J. Meyer and N. Y. Murakami Iha, *Inorg. Chem.*, 2014, **53**, 4089-4099.
53. B. Carlson, G. D. Phelan, W. Kaminsky, L. Dalton, X. Z. Jiang, S. Liu and A. K.-Y. Jen, *J. Am. Chem. Soc.*, 2002, **124**, 14162.
54. J. V. Caspar, T. D. Westmoreland, G. H. Allen, P. G. Bradley, T. J. Meyer and W. H. Woodruff, *J. Am. Chem. Soc.*, 1984, **106**, 3492.
55. J. A. Treadway, B. Loeb, R. Lopez, P. A. Anderson, F. R. Keene and T. J. Meyer, *Inorg. Chem.*, 1996, **35**, 2242.
56. N. H. Damrauer, T. R. Boussie, M. Devenney and J. K. McCusker, *J. Am. Chem. Soc.*, 1997, **119**, 8253.
57. K. E. Spettel and N. H. Damrauer, *J. Phys. Chem. A*, 2014, **118**, 10649-10662.
58. P. C. Alford, M. J. Cook, A. P. Lewis, G. S. G. McAuliffe, V. Skarda, A. J. Thomson, J. L. Glasper and D. J. Robbins, *J. Chem. Soc. Perkin Trans. 2*, 1985, 705.
59. Y.-L. Chen, S.-W. Lee, Y. Chi, K.-C. Hwang, S. B. Kumar, Y.-H. Hu, Y.-M. Cheng, P.-T. Chou, S.-M. Peng, G.-H. Lee, S.-J. Yeh and C.-T. Chen, *Inorg. Chem.*, 2005, **44**, 4287.
60. Z. Deng, S. T. Lee, D. P. Webb, Y. C. Chan and W. A. Gambling, *Synth. Met.*, 1999, **107**, 107-109.
61. S.-J. Su, D. Tanaka, Y.-J. Li, H. Sasabe, T. Takeda and J. Kido, *Org. Lett.*, 2008, **10**, 941.
62. A. Endo, K. Sato, K. Yoshimura, T. Kai, A. Kawada, H. Miyazaki and C. Adachi, *Appl. Phys. Lett.*, 2011, **98**, 083302.
63. C.-H. Chang, C.-L. Ho, Y.-S. Chang, I.-C. Lien, C.-H. Lin, Y.-W. Yang, J.-L. Liao and Y. Chi, *J. Mater. Chem. C*, 2013, **1**, 2639.
64. Y. Hamada, H. Kanno, T. Tsujioka, H. Takahashi and T. Usuki, *Appl. Phys. Lett.*, 1999, **75**, 1682.
65. S. C. Tse, K. C. Kwok and S. K. So, *Appl. Phys. Lett.*, 2006, **89**, 262102.

66. J. Lee, J.-I. Lee, K.-I. Song, S. J. Lee and H. Y. Chu, *Appl. Phys. Lett.*, 2008, **92**, 133304.
67. Y.-L. Tung, S.-W. Lee, Y. Chi, Y.-T. Tao, C.-H. Chien, Y.-M. Cheng, P.-T. Chou, S.-M. Peng and C.-S. Liu, *J. Mater. Chem.*, 2005, **15**, 460.
68. T.-H. Liu, S.-F. Hsu, M.-H. Ho, C.-H. Liao, Y.-S. Wu, C. H. Chen, Y.-L. Tung, P.-C. Wu and Y. Chi, *Appl. Phys. Lett.*, 2006, **88**, 063508.
69. C.-H. Chien, F.-M. Hsu, C.-F. Shu and Y. Chi, *Org. Electron.*, 2009, **10**, 871.
70. J. Kalinowski, M. Cocchi, V. Fattori, L. Murphy and J. A. G. Williams, *Org. Electron.*, 2010, **11**, 724-730.
71. S.-J. Su, E. Gonmori, H. Sasabe and J. Kido, *Adv. Mater.*, 2008, **20**, 4189.
72. H. Sasabe, J.-i. Takamatsu, T. Motoyama, S. Watanabe, G. Wagenblast, N. Langer, O. Molt, E. Fuchs, C. Lennartz and J. Kido, *Adv. Mater.*, 2010, **22**, 5003.
73. M. A. Baldo, C. Adachi and S. R. Forrest, *Phys. Rev. B.*, 2000, **62**, 10967.
74. D. Hertel and K. Meerholz, *J. Phys. Chem. B*, 2007, **111**, 12075-12080.
75. S. Reineke, K. Walzer and K. Leo, *Phys. Rev. B.*, 2007, **75**, 125328.
76. H.-H. Yeh, S.-T. Ho, Y. Chi, J. N. Clifford, E. Palomares, S.-H. Liu and P.-T. Chou, *J. Mater. Chem. A*, 2013, **1**, 7681.
77. L. Porrès, A. Holland, L.-O. Pålsson, A. Monkman, C. Kemp and A. Beeby, *J. Fluoresc.*, 2006, **16**, 267-273.
78. A. K. Gaigalas and L. Wang, *J. Res. Natl. Inst. Stand. Technol.*, 2008, **113**, 17-28.
79. A. D. Becke, *J. Chem. Phys.*, 1993, **98**, 5648.
80. P. J. Stephens, F. J. Devlin, C. F. Chabalowski and M. J. Frisch, *J. Phys. Chem.*, 1994, **98**, 11623-11627.
81. P. J. Hay and W. R. Wadt, *J. Chem. Phys.*, 1985, **82**, 299.
82. G. A. Petersson and M. A. Al-Laham, *J. Chem. Phys.*, 1991, **94**, 6081.
83. N. M. O'Boyle, A. L. Tenderholt and K. M. Langner, *J. Comp. Chem.*, 2008, **29**, 839.



Os(II) complexes bearing chromophoric 1,10-phenanthroline, diphosphine and bipyrazolate ancillaries display efficient NIR emission ranging from 717 nm to 779 nm in the solid state at RT.